Environmental Pollution 295 (2022) 118690

Contents lists available at ScienceDirect

Environmental Pollution

journal homepage: www.elsevier.com/locate/envpol

Legislative and functional aspects of different metrics used for ozone risk assessment to forests

Alessandro Anav [a], Alessandra De Marco [a,*], Alessio Collalti [b], Lisa Emberson [c], Zhaozhong Feng [d], Danica Lombardozzi [e], Pierre Sicard [f], Thomas Verbeke [g], Nicolas Viovy [h], Marcello Vitale [i], Elena Paoletti [j]

[a] Department of Sustainability, Italian National Agency for New Technologies, Energy and the Environment (ENEA), Rome, Italy
[b] Forest Modelling Laboratory. Institute for Agriculture and Forestry Systems in the Mediterranean, National Research Council of Italy (CNR–ISAFOM), Perugia, Italy
[c] Environment and Geography Department, University of York, York, UK
[d] Institute of Ecology, School of Applied Meteorology, Nanjing University of Information Science & Technology, Nanjing, China
[e] Climate and Global Dynamics, National Center for Atmospheric Research (NCAR), Boulder, CO, USA
[f] ARGANS, Biot, France
[g] Laboratory of Mechanics and Technology, ENS Paris-Saclay, Gif sur Yvette, France
[h] Laboratory for Sciences of Climate and Environment (LSCE), Gif sur Yvette, France
[i] Department of Environmental Biology, Sapienza University, Rome, Italy
[j] Institute of Research on Terrestrial Ecosystems, National Research Council of Italy (CNR–IRET), Sesto Fiorentino, Italy

ARTICLE INFO

Keywords:
Tropospheric ozone
Northern hemisphere
Ozone risk assessment
Forests
Process based models
Chemical transport models

ABSTRACT

Surface ozone (O_3) is a threat to forests by decreasing photosynthesis and, consequently, influencing the strength of land carbon sink. However, due to the lack of continuous surface O_3 measurements, observational-based assessments of O_3 impacts on forests are largely missing at hemispheric to global scales.

Currently, some metrics are used for regulatory purposes by governments or national agencies to protect forests against the negative impacts of ozone: in particular, both Europe and United States (US) makes use of two different exposure-based metrics, i.e. AOT40 and W126, respectively. However, because of some limitations in these metrics, a new standard is under consideration by the European Union (EU) to replace the current exposure metric.

We analyse here the different air quality standards set or proposed for use in Europe and in the US to protect forests from O_3 and to evaluate their spatial and temporal consistency while assessing their effectiveness in protecting northern-hemisphere forests. Then, we compare their results with the information obtained from a complex land surface model (ORCHIDEE).

We find that present O_3 uptake decreases gross primary production (GPP) in 37.7% of the NH forested area of northern hemisphere with a mean loss of 2.4% year^{-1}. We show how the proposed US (W126) and the currently used European (AOT40) air quality standards substantially overestimate the extension of potential vulnerable regions, predicting that 46% and 61% of the Northern Hemisphere (NH) forested area are at risk of O_3 pollution. Conversely, the new proposed European standard (POD1) identifies lower extension of vulnerability regions (39.6%).

1. Introduction

During the 20th century, atmospheric pollution increased significantly over large regions of the northern hemisphere (Young et al., 2013) because of increasing anthropogenic emissions from both industrialized and developing countries (Hartmann et al., 2013). The rapid increase in the concentration of air pollutants has thus posed new scientific and political challenges to protect forests from atmospheric pollution, which was identified as an unfavourable condition for vegetation growth (Johnson and Siccama, 1983). Tropospheric ozone (O_3) is a short-lived trace gas that either originates in the stratosphere and is then transported toward the lower atmosphere (i.e. troposphere) or is

* Corresponding author.
E-mail address: alessandra.demarco@enea.it (A. De Marco).

https://doi.org/10.1016/j.envpol.2021.118690
Received 22 November 2021; Received in revised form 9 December 2021; Accepted 13 December 2021
Available online 15 December 2021

produced in-situ by photochemical reactions among precursors such as nitrogen oxides (NOX), carbon monoxide (CO), methane (CH4) and volatile organic compounds (VOCs) as well as peroxyacetyl nitrate (PAN) (Milford et al., 1994; Fischer et al., 2014; Monks et al., 2015).

Ozone is harmful for vegetation as it impairs photosynthesis and plant growth with consequences for the terrestrial land carbon sink and ecosystem health (Reich and Amundson, 1985; Sitch, 2007). Several studies display a substantial effect of O_3 on forest primary production (Lombardozzi et al., 2015; Yue and Unger, 2018), although the quantification of ozone-induced photosynthesis loss is often ignored or poorly represented in most of the global land carbon assessments (Canadell, 2021). A prompt identification of potential vulnerable forests to air pollution is crucial to develop effective mitigation and adaptation strategies able to prevent effects ranging from long-term damages to forest mortality (Forzieri et al., 2021). Unfortunately, observational-based studies addressing O_3 damage to photosynthesis mostly remain site-level and are limited by the sparse number of sites where both air quality and eddy covariance measurements are available (Yue & Unger, 2014; Fares et al., 2013; Verrickt et al., 2017; Yue et al., 2016). Consequently, large scale assessments of O_3 threat to forests are necessarily performed with complex process-based models (Sitch et al., 2007; Lombardozzi et al., 2015; Yue and Unger, 2018) which account for the biological, physical and chemical processes affecting O_3 uptake into vegetation and the consequent effects on plant physiology. Alternatively, some metrics have been developed to quickly identify forest areas potentially vulnerable to O_3 stress (Lefhon et al., 2018; Mills et al., 2018; Musselman et al., 2006), and estimate the consequent plant response using some simple dose-response relationships inferred from field experiments (Mills et al., 2011a,b). Yet, it is still challenging to understand how well these metrics can identify vulnerable forests and whether they agree with estimates from process-based models.

Sitch et al. (2007) estimated the impact of projected changes in O_3 levels on the land-carbon sink, using a global land carbon cycle model, which accounted for both the effect of O_3 on photosynthesis and the interactions between O_3 and CO_2 through stomatal closure; it was showed that, because of O_3 stress on plants, gross primary production (GPP) was projected to decrease over the time period 1901–2100 by 14–23% with some regional peaks even above 30% (Sitch et al., 2007).

The magnitude of O_3 stress to forests was quantified in several modelling studies ranging from regional (Anav et al., 2011; Sun et al., 2012; Yue and Unger, 2014; Franz et al., 2017; Verryckt et al., 2017; Yue et al., 2017; Franz et al., 2018; Oliver et al., 2018; Park et al., 2018) to global (Lombardozzi et al., 2012, 2015; Sicard et al., 2017) as well as in many field experiments (Matyssek et al., 2010b; Pretzsch et al., 2010; Hoshika et al., 2012, 2015; Fares et al., 2013; Braun et al., 2014; Talhelm et al., 2014; Kitao et al., 2016; Proietti et al., 2016; Sicard et al., 2016; Yue et al., 2016). Some meta-analysis and review papers summed up all the available information from the literature (e.g. Matyssek et al., 2010a; Leisner and Ainsworth, 2012; Ainsworth et al., 2012; Lombardozzi et al., 2013; Fuhrer et al., 2016; Agathokleous et al., 2016; Jolivet et al., 2016; Li et al., 2017; Cailleret et al., 2018).

In contrast to process-based models, which estimate and quantify the O_3 damage to plants using complex biogeochemical parameterization, since the '90s several O_3 metrics have been developed (Musselman et al., 2006); these metrics were simpler than process-based models, and allowed to estimate the O_3 exposure or uptake by plants and quantify the consequent plant response by simple dose-response relationships inferred from field experiments (e.g. Mills et al., 2011a).

Despite at local/regional scale the current state of knowledge of O_3 metrics of relevance to vegetation has already been discussed in several papers (Musselman et al., 2006; Karlsson et al., 2007; Paoletti et al., 2007; Simpson et al., 2007; De Marco et al., 2015, 2020; Lefohn et al., 2018; Mills et al., 2018), at larger scale (i.e. hemispheric to global) the information on the potential O_3 risk to forests is very limited. In fact, in most of the previous risk assessment studies based on measurements only (e.g. Lefohn et al., 2018; Mills et al., 2018), the information on the potential O_3 risk to forests was limited by the data availability, leading to an insufficient knowledge in sparsely populated regions where surface air quality measurements were missing. For this reason, the quantification of large-scale damage is exclusively performed through models. However, one of the main limitations related to models is the generally coarse spatial resolution of chemistry models used to produce O_3 data (e.g. Simpson et al., 2007; Colette et al., 2012; Hoshika et al., 2015; Monks et al., 2015; Sicard et al., 2017), which poorly reproduce the local variability of air pollutants especially in complex highly polluted regions where emissions and transport of pollutants, away from the source of emission, play a pivotal role in determining air quality (Li et al., 2014; Strode et al., 2015; Huang et al., 2017; Jonson et al., 2018). The present availability of a regional coupled chemistry-climate model (i.e. WRF-Chem) with a fine spatial resolution (~25 km), covering most of the northern hemisphere (NH) (Grell et al., 2005), allows to overcome the spatial resolution limitation.

The aim of this study was to compare European and US air quality metrics used for ozone risk assessment for forest trees, in terms of geographical distribution and in terms of exceedance of the critical levels. Because of the difficulties associated to the computation of ozone uptake by plants, which requires several meteorological data in addition to the O_3 concentrations, these metrics has been neglected in previous ozone risk assessments for forests at large scale (i.e. from hemispheric to global). To compute the different metrics, we used results from WRF-Chem for NH. Noteworthy, current surface O_3 concentrations are still high enough to damage NH forests, despite the successful control policies to reduce O_3 precursors emissions (Anav et al., 2019; Unger et al., 2020). Then, we quantified the effect of O_3 on GPP, and compared the estimated damage with the information obtained from the different metrics. We postulated that exposure-based metrics (AOT40 and W126, respectively) overestimate O3 risk to forests relative to the uptake metric (POD1), and we aimed at quantifying this overestimation for the entire NH.

2. Materials and methods

2.1. WRF-chem model

Hourly O_3 concentrations and meteorological variables used to compute the different metrics presented in this study were simulated by the Weather Research and Forecasting model with Chemistry (WRF-Chem, version 3.9). The WRF model is a limited-area, non-hydrostatic, terrain-following eta-coordinate mesoscale model (Skamarock and Klemp, 2008); this model has been further developed to include various gas-phase chemistry and aerosol mechanisms creating the coupled chemistry-climate WRF-Chem model (Grell et al., 2005).

The WRF model system offers multiple options for various physical packages (Skamarock and Klemp, 2008). The dynamical core used in this work is the Advanced Research Weather Research and Forecasting model; we used a single-moment 6-class scheme to resolve the microphysics (Hong and Lim, 2006) and the Rapid Radiative Transfer Model for GCMs (RRTMG) for the shortwave and longwave radiation (Iacono et al., 2008). Convective precipitation and cumulus parameterization were resolved with the new Tiedtke scheme (Zhang et al., 2011), the planetary boundary layer computations were performed using the nonlocal K-profile Yongsei University parameterization (Hong and Lim, 2006), while the exchange of heat, water and momentum between soil-vegetation and atmosphere was simulated by the Unified Noah Land Surface Model (Chen and Dudhia, 2001).

Similarly to physical parameterizations, many different gas phase chemistry and aerosol options are available in WRF-Chem. In this study, gas-phase chemical reactions are calculated using the chemical mechanism MOZART (*Model for OZone And Related chemical Tracers*) (Emmons et al., 2010) whereas for the aerosols we used the GOCART (*Global Ozone Chemistry Aerosol Radiation and Transport*) bulk aerosol approach (Chin et al., 2000). This set-up includes 85 gas-phase species, 12 bulk

aerosol compounds, 39 photolysis and 157 gas-phase kinetic reactions.

Anthropogenic emissions are based on the EDGAR-HTAP (*Emission Database for Global Atmospheric Research for Hemispheric Transport of Air Pollution*) global emission inventory which includes emissions of gaseous pollutants such as SO_2, NO_x, CO, non-methane volatile organic compounds (NMVOCs), NH_3 black carbon and particulate matter. Fire emissions are provided using the FINN (Fire INventory from NCAR) inventory (Wiedinmyer et al., 2011); this dataset provides estimates of trace gases and particles emitted by open biomass burning at ~1 km resolution. Biogenic emissions are calculated online using the MEGAN (Model of Emissions of Gases and Aerosols from Nature) model (Guenther et al., 2006).

The initial and boundary meteorological conditions (including time varying sea surface temperature), required to run the model, are provided by the European Centre for Medium-range Weather Forecast (ECMWF) re-analysis project ERA5 (Hersbach et al., 2020), with a horizontal resolution of ~31 km every 3 h. Similarly, MOZART-4/Goddard Earth Observing System Model version 5 (GEOS-5) data were used for chemical and aerosol boundary conditions. The MOZART-4 data is a model output dataset available at a horizontal grid resolution of $1.9^{\circ} \times 2.5^{\circ}$ every 6 h and is driven by the National Aeronautics and Space Administration (NASA) GEOS-5 model.

For validating the model results over different seasons and regions, we used the year 2016, when measurements from rural sites (e.g. EPA, NAPS, CASTNet, EEA, Airbase, EMEP, GAW networks), i.e. representative of background O_3 conditions (de Leeuw, 2000), were available ((Sofen et al., 2016a,b). Considering both the moderate inter-annual variations in O_3-induced GPP changes (Yue, 2018) and the low spatial and temporal variability of metrics (Anav et al., 2016), the results and conclusions from this study are expected to apply more broadly over other years.

To estimate distribution and type of forest over the hemispheric domain, the U.S. Geological Survey (USGS) Global Land Cover Characterization (GLCC) dataset (Loveland et al., 2000) and the Köppen-climate classification (Kottek et al., 2006) were used to link USGS vegetation to bio-climatic ranges (Anav et al., 2018).

2.2. Impact of O_3 on GPP from ORCHIDEE

To quantify changes in photosynthesis caused by O_3, we use the ORCHIDEE "ORganizing Carbon and Hydrology in Dynamic EcosystEms" model (Musselman et al., 2006) driven by meteorological data and O_3 concentrations simulated by the WRF-Chem model (year 2016). ORCHIDEE simulates fluxes of carbon, water and energy between the atmosphere and land surface. As most of the process-based models, in ORCHIDEE the carbon assimilation scheme is simulated using the coupled Farquhar (Farquhar et al., 1980) biochemical photosynthesis model and Ball–Berry stomatal conductance model (Krinner et al., 2005). To represent the effects of O_3 on vegetation functioning, we added into ORCHIDEE a damage function (f_{O3}). This function is based on the O_3 flux entering the leaves, thus it reproduces the typical observed non-linear reduction of photosynthesis and stomatal conductance in response to damaging ambient levels of O_3, taking also into account the detoxification processes. At each time step, the instantaneous damaging flux $FO3_Y$ [nmol m^{-2} s^{-1}] is calculated as follows:

$$FO3_Y(t) = Gs_{O_3}(t) \cdot O_3(t) - FO3_{td} f_{age}(t) \quad (1)$$

where $Gs_{O3}(t)$ represents the stomatal conductance to O_3 (in mmol m^{-2} s^{-1}), $O_3(t)$ is the near-surface O_3 concentration (in ppb), $FO3_{td}$ is the threshold flux prescribed to the value Y (in nmol m^{-2} s^{-1}) and the scalar factor $f_{age}(t)$ which is the senescence factor depending on the leaf age and varying between 0 and 1. The latter describes the dynamic impact of the senescence on the detoxification ability, which is maximal for young leaves ($f_{age} = 1$) and decreases with the leaf age ($f_{age} = 0$) up to zero. Following the recommendations of CLRTAP (2017), the value Y of the threshold flux for forests is set to 1 nmol m^{-2} s^{-1}. From the instantaneous damaging flux, the phytotoxic O_3 dose $POD_Y(t)$ is computed by integrating $FO3_Y$ between the start of growing plant season (SOS) and the given time step t:

$$POD_Y(t) = \int_{SOS}^{t} FO3_Y(t)dt \quad (2)$$

where Y refers to the value of the constant threshold flux $FO3_{td}$. Besides, in order to represent the observed delay in the effects on photosynthesis, we added the threshold parameter POD_c (in mmol m^{-2} s^{-1}), which corresponds to the phytotoxic O_3 dose above which the photosynthesis starts to decrease due to the effective O_3 damages inside the leaf. Finally, we compute the damage scalar factor f_{O3} at each time step by solving the following equation:

$$\frac{\partial f_{O3}(t)}{\partial t} = -\beta f_{O3}(t)(POD(t) - POD_c)FO3_Y(t) \quad (3)$$

where β is a plant-specific empirical coefficient of sensitivity. The solution $f_{O3}(t)$ displays the typical curvilinear response of photosynthesis commonly observed during fumigation experiments on various species sensitive to O_3 (Novak et al., 2005; Pell et al., 1992). The parameters β and POD_c were calibrated using hourly meteorological data and O_3 concentration from fumigation experiments conducted on several tree species (Novak et al., 2005; Hoshika et al., 2012; Kronfuβ et al., 1998).

2.3. Air quality metrics

According to the EU Directive on Ambient Air Quality and Cleaner Air (2008/50/EC), the air quality standard used for vegetation in Europe is the Accumulated Ozone over a Threshold of 40 ppb (AOT40, in ppb h); it is computed as the sum of the hourly exceedances above 40 ppb between 8AM and 8PM and is cumulated over the period 1st April-30th September:

$$AOT40 = \int_{t=1^{st}April}^{30^{th}September} \max\left([O_3]_t - 40, 0\right)dt \quad (4)$$

where $[O_3]$ is the mean hourly O_3 concentration (ppb) estimated through WRF-Chem model and *dt* is the time step (1 h); the function "maximum" ensures that only values exceeding 40 ppb are included.

The US Environmental Protection Agency (EPA) proposed for use as a secondary air quality standard the W126 metric. The W126 (ppb h) is computed as the sigmoidal weighting sum of hourly O_3 concentrations between 8AM and 8PM and, for consistency of analysis, was cumulated over the same temporal period of AOT40:

$$W126 = \int_{t=1^{st}April}^{30^{th}September} \frac{[O_3]_t}{1 + 4403e^{\left(-0.126[O_3]_t\right)}}dt \quad (5)$$

where [O3] is the hourly O3 concentration (ppb) simulated by WRF-Chem model and dt is the time step (1 h). The weighting function is used to assign greater emphasis to higher O_3 concentrations (Lefohn et al., 2018).

According to the EU Directive on Ambient Air Quality and Cleaner Air (2008/50/EC) the critical level set for forest protection is 9 ppm h AOT40, while for W126 we considered 7 ppm h and 21 ppm h for sensitive and tolerant forests (Heath et al., 2009), respectively.

These standards have the same flaw, namely, they do not consider any environmental stress to vegetation, therefore, a different ozone-risk metric has been developed, that is based on cumulated stomatal flux above a given phytotoxic threshold below which plants are able to detoxify ozone (Emberson et al., 2000).

The stomatal O_3 uptake, with a Y threshold of 1 nmol m^{-2} s^{-1} (i.e. POD_1), is expressed as follows (CLRTAP, 2017):

$$POD_1 = \int_{t=SGS}^{EGS} \max\left([O_3]_t * g_{sto} * \frac{R_c}{R_c + R_b} - 1, 0\right) dt \quad (6)$$

where $[O_3]$ is the hourly O_3 concentration (ppb), R_b is the quasi-laminar resistance (s m^{-1}), R_c is the leaf surface resistance (s m^{-1}), g_s is the stomatal conductance to O_3 (mmol O_3 m^{-2} s^{-1}), and SGS (start of growing season) and EGS (end of growing season) represent the beginning and the end of plant growing season, respectively. Note that AOT40 and W126 are cumulated between 1st April-30th September 2016, while POD_1 is cumulated over the specific forest type growing season length estimated from satellite leaf area index (LAI) as in Anav et al. (2018).

The stomatal conductance is computed using the Jarvis's algorithm (Jarvis, 1976) which describes the species-specific effects of soil water availability, vapour pressure deficit, air temperature, and solar radiation on stomatal functioning. The leaf-level stomatal conductance (g_s, in mmol O_3 m^{-2} s^{-1}) is estimated as follows:

$$g_{sto} = g_{max} * f_{phen} * f_{light} * \max\left(f_{min}, f_{temp} * f_{VPD} * f_{SWC}\right) \quad (7)$$

where g_{max} is the maximum stomatal conductance of a plant species (mmol O_3 m^{-2} PLA s^{-1}), f_{min} is the minimum stomatal conductance expressed as a fraction of g_{max}, while the functions f_{light} (Eq. (8)), f_{temp} (Eq. (9)), f_{VPD} (Eq. (10)), and f_{SWC} are scalar species–specific factors describing limitation ($f_x = 0$) or not limitation ($f_x = 1$) to maximum stomatal conductance because of photosynthetically photon flux density at the leaf surface (PPFD), surface air temperature (T), vapour pressure deficit (VPD), and volumetric soil water content (SWC). Finally, the f_{phen} function is used to define the duration of the growing season during which plants can uptake O_3; we used LAI seasonal variations to compute the SGS and EGS, as described in Anav et al. (2018).

These scaling factors are defined as follows (CLRTAP, 2017):

$$f_{light} = 1 - e^{(-light_a * PPFD)} \quad (8)$$

$$f_{temp} = \max\left(f_{min}, \left(\frac{T - T_{min}}{T_{opt} - T_{min}}\right) * \left(\frac{T_{max} - T}{T_{max} - T_{opt}}\right)^{\left(\frac{T_{max} - T_{opt}}{T_{opt} - T_{min}}\right)}\right) \quad (9)$$

$$f_{VPD} = \min\left\{1, \max\left[f_{min}, \left(\frac{(1 - f_{min}) * (VPD_{min} - VPD)}{VPD_{min} - VPD_{max}}\right) + f_{min}\right]\right\} \quad (10)$$

$$f_{SWC} = \min\left[1, \max\left(f_{min}, \frac{SWC - WP}{FC - WP}\right)\right] \quad (11)$$

where light is a dimensional constant, PPFD is hourly photosynthetic photon flux density (μmol photons m^{-2} s^{-1}), T_{opt}, T_{min}, and T_{max} () represent the optimum, minimum, and maximum temperature (T, °C) for g_{sto}, VPD_{min} and VPD_{max} (kPa) are minimum and maximum VPD for g_{sto}, and WP and FC are the soil water content (m^3 m^{-3}) at wilting point and field capacity, respectively (CLRTAP, 2017).

It should be noted that stomatal conductance depends on the vegetation type, thus land cover is a key variable when computing POD_1 as each vegetation category has specific properties and ranges for the stomata opening controlled by the above mentioned limiting functions.

For the POD_1 critical levels we used 5.2 mmol m^{-2} y^{-1} for boreal and continental deciduous forests, 9.2 mmol m^{-2} y^{-1} for boreal and continental evergreen forests, 14 mmol m^{-2} y^{-1} for temperate deciduous forests and 47.3 mmol m^{-2} y^{-1} for temperate evergreen forests (CLRTAP, 2017).

3. Results and discussion

3.1. Distribution of ozone concentrations

During spring (i.e. March-April-May), the O_3 concentration shows maximum values (>40 ppb) over Greenland, Tibetan plateau and in the arctic regions (e.g. Alaska and Siberia), whereas, in the polluted areas of central Europe, the eastern US and south-eastern Asia O_3 has its minimum (<30 ppb) because of night-time titration by NO and weak photolysis rates (Fig. 1). The high concentrations observed over Greenland are due to i) O_3 formation attributed to local sources like NO_x enhancement from snowpack emissions, ii) thermal decomposition of PAN and iii) ship emissions (Law and Stohl, 2007; Walker et al., 2012). In addition, the long-range transport of O_3 and its precursors from Europe and North America as well as stratospheric O_3 inputs, associated with low deposition rates, contribute to O_3 peaks over Greenland. Similarly, for latitudes over 60°N, air pollutants are transported to the Arctic, primarily from Eurasia, North America and Asia leading to high O_3 concentrations (namely Arctic haze) in early spring when the dry deposition is low (Law and Stohl, 2007). On the other side, the large O_3 concentrations observed over the Tibetan plateau are attributed to the combined effects of: i) the elevation and high ice/snow reflectance, which lead to a larger amount of available UV radiation, thus increasing the photochemical reaction rates; ii) the strong thermal and dynamical forcing of the Tibetan plateau on regional climate associated with the large–scale circulation; iii) the local production favoured by the significant amount of O_3 precursors transported from surrounding polluted regions (Tian et al., 2008; Guo et al., 2015; Wang et al., 2015; Sicard et al., 2017).

During the summer season (June-July-August), the larger surface O_3 concentrations are observed over the Tibetan plateau, Greenland, western and eastern U.S and in a latitudinal range between 15° and 45°N, while lower O_3 concentrations are found over Canada, South Asia and regions over latitude 60°N. The maxima found at northern mid-latitudes are attributed to the peak in local and regional photochemical O_3 production promoted by high solar radiation, increased daylight period and forest fire emissions (Andreae and Merlet, 2001; Mavrakis et al., 2010c; Parrish et al., 2013; Li et al., 2014), while the O_3 minimum in the boreal region are related to the high deposition rates to forests and the advection of clean air-masses from the Arctic and the Pacific Ocean.

During autumn (September-October-November), O_3 has the higher concentrations over Greenland, Tibetan plateau and regions with desert and ice as well as in the western US, while minimum O_3 concentrations are found in central Europe and south-eastern Asia due to the O_3 titration under high NO_x levels. In fact, the fresh emissions of NO, occurring during the colder months in the polluted regions, rapidly react with O_3 to produce NO_2 (Doherty et al., 2005; Bloomer et al., 2010; Monks et al., 2015), while the NO_2 reactions are limited by low solar radiation.

In general, chemical transport models well reproduce the seasonal variability and spatial pattern of mean O_3 concentrations at regional–to–global scale, and they are able to simulate the higher O_3 levels in areas downwind of precursor sources and at the high–elevation and remote areas (Lin et al., 2012; Lamarque et al., 2013; Sicard et al., 2017). Unfortunately, the availability of in-situ measurements is limited to populated regions only, while satellite data provides information on the total column content or the lowermost troposphere, thus they are poorly representative of the surface layer (Cuesta et al., 2018). Nevertheless, a broad number of air quality measurements from several monitoring stations are available for validating our results (e.g. Schultz et al., 2017; Gaudel et al., 2018; Tarasick et al., 2019); these measurements have a heterogeneous spatial distribution covering different region of the globe with different meteorological and climatic conditions (Fig. 2).

Overall, the model well reproduces the seasonal variability in surface O_3 in US, Europe and over Asia during summer, while discrepancies can be observed during spring and autumn, mainly over China or near the Mediterranean coastal sites. Compared to ground observations, the WRF-Chem model overestimates O_3 concentrations across Europe, US and Asia: the absolute mean (i.e. unsigned) bias is 9 ppb for the US (658 sites), 4.6 ppb for Europe (563 sites) and 9.7 ppb over Asia (607 sites). The observed bias is mainly attributed to the large uncertainty in the anthropogenic emissions (Parrish et al., 2014; Oikonomakis et al.,

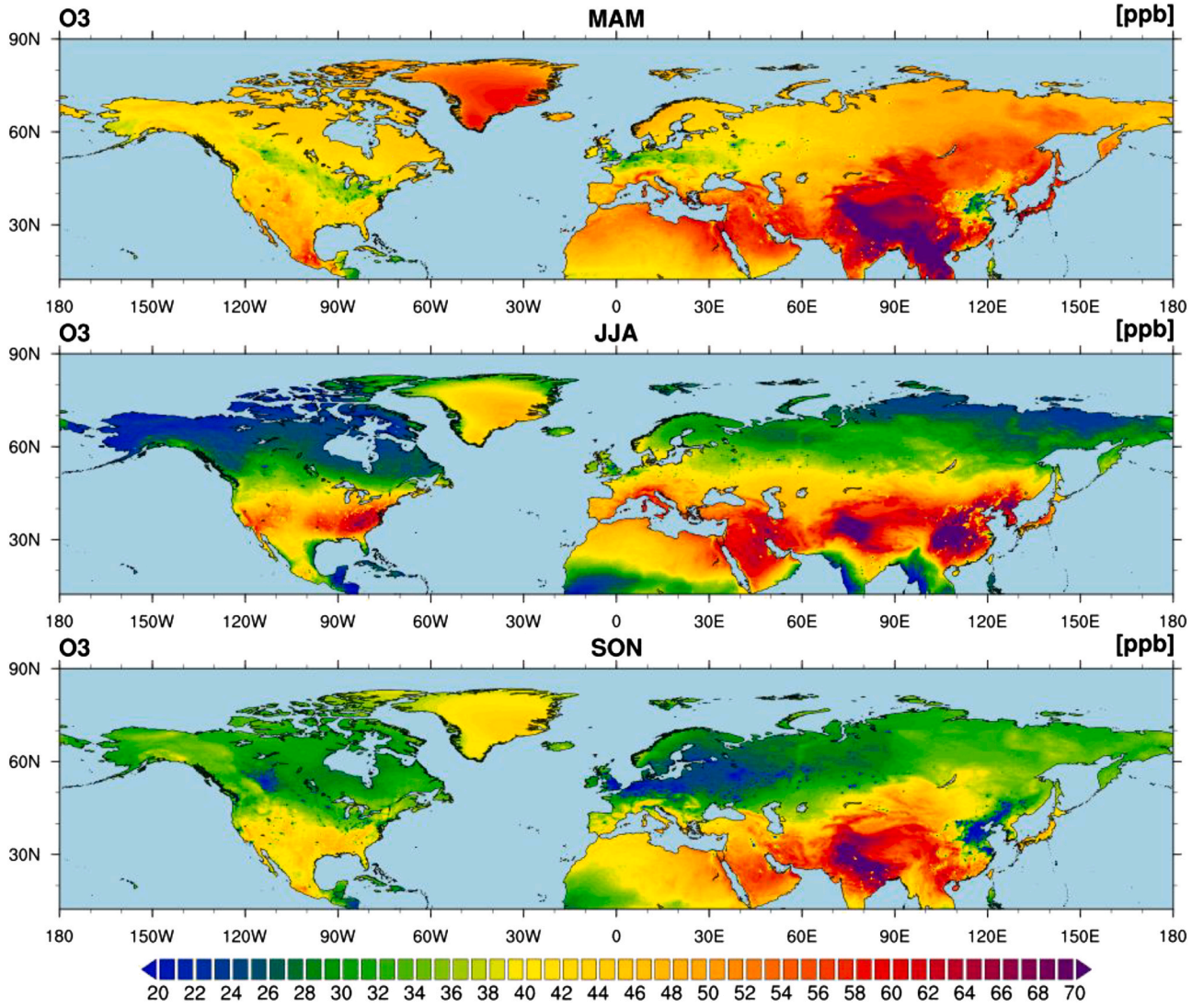

Fig. 1. Spatial distribution of WRF-Chem simulated mean daily surface ozone concentrations over land areas of northern hemispere during different seasons (i.e. March-April-May; June-July-August; September-October-November) in 2016.

2018), which are not updated to the year 2016 (Georgiou et al., 2018) and the coarse parameterization of dry deposition through plant stomata (Rydsaa et al., 2016). On the other side, WRF-Chem well reproduces the observed spatial and seasonal variability of the relevant meteorological variables affecting surface air chemistry and required in the following sections to estimate the amount of ozone taken up by forests (**see** supporting **information**).

3.2. Air quality standards used for forest protection

Air quality standards have been established to prevent or minimize the risk of adverse effects to forest health from air pollution. As these standards are often used in conjunction with statistically-derived critical levels (Fuhrer et al., 1997; Ashmore et al., 2004; Mills et al., 2011a), i.e. threshold values above which detrimental effect on forest may occur, their spatial distribution provides a valuable tool to prevent long-term injury to trees (Musselman et al., 2006).

Generally, two groups of metrics have been developed; the first group, defined as exposure-based metrics, considers the adverse effects of ozone to vegetation to be dependent on the canopy O_3 concentration only, following the rather simple rationale that higher O_3 concentrations is assumed to be more damaging to plants (Simpson et al., 2007). In the second group, defined as flux-based metrics, the risk depends on the amount of O_3 entering the leaves through the stomata (i.e. uptake).

The European standard used to protect vegetation against negative impacts of ozone is the Accumulated Ozone over a Threshold of 40 ppb, i.e. AOT40 (EU Directive on Ambient Air Quality and Cleaner Air, 2008/50/EC); it is a concentration-based metric that describes the hourly O_3 accumulated exposure of forests. Exposure is generally limited to the period when stomata are open, thus AOT40 is, for simplicity, calculated over the daylight hours (8AM-8PM) during the plant growing season (CLRTAP, 2017); the critical level value set for forest protection, computed during the time window 1st April– 30th September, is 9 ppm h (Directive, 2008/50/EC) (Paoletti et al., 2014; Lefohn et al., 2018; Mills et al., 2018).

The US Environmental Protection Agency (EPA) uses the W126 metric to protect vegetation from ozone damage (US EPA, 2013; 2014a; US Federal Register, 2015). The W126 is an exposure-based metric calculated from the sum of hourly O_3 concentrations, weighted by a sigmoidal function ranging from 0 to 1, during daylight hours through the plant growing season. The sigmoidal weighting function is used to give more weight to higher O_3 concentrations. The W126 can be accumulated over 3, 6, 7 and 12 months (Lefohn et al., 2018; Mills et al., 2018). In case of sensitive tree species, the critical level is 7 ppm h, while for tolerant species the threshold is 21 ppm h (EPA, 2007; Paoletti et al., 2014; Mills et al., 2018).

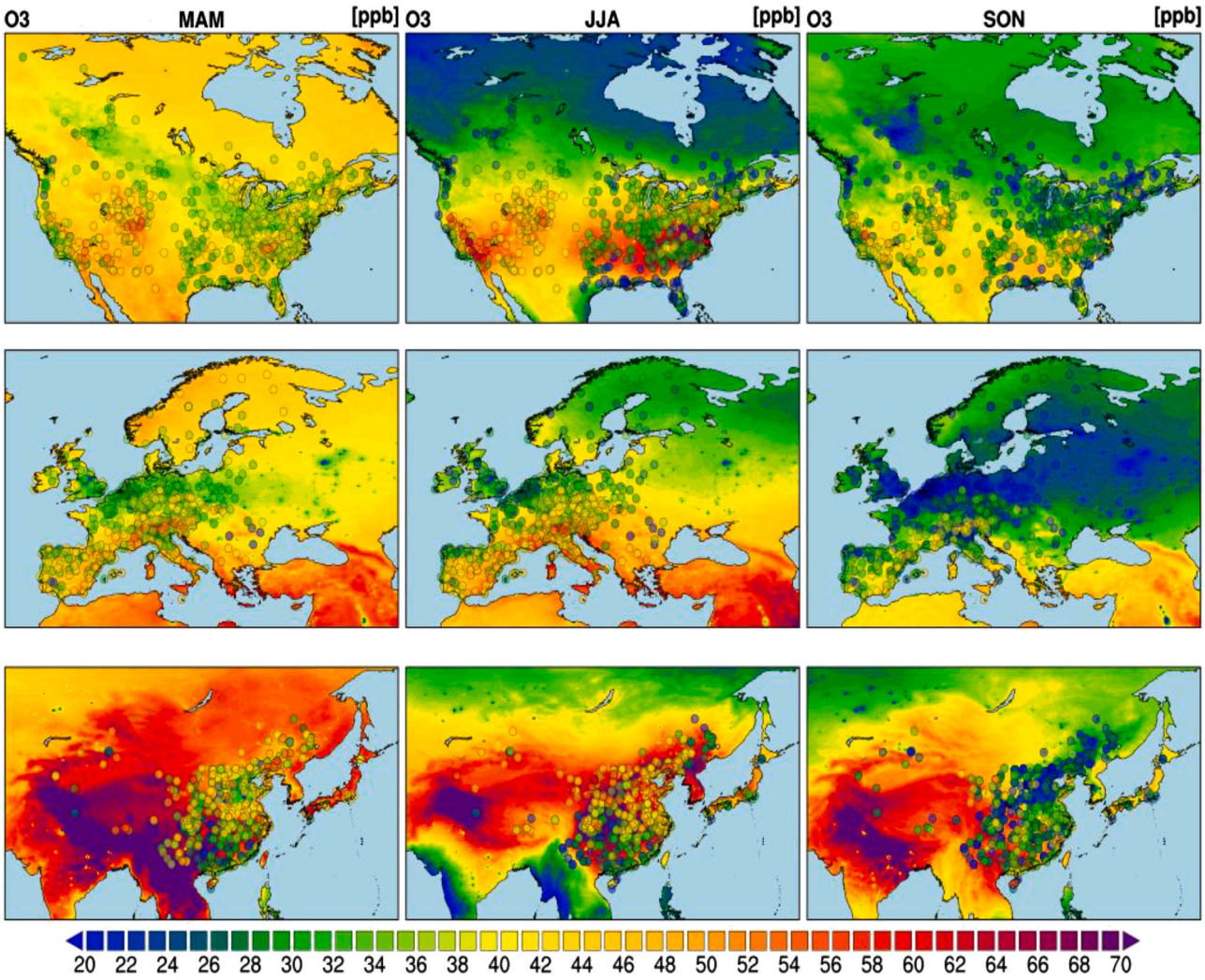

Fig. 2. Comparison of simulated mean daily surface ozone concentrations averaged over different seasons for US, Europe and eastern Asia with in-situ observations (dots).

As already reported by Mills et al. (2018), the European and US standards have some points in common: firstly, the higher is the ozone concentration the larger is the magnitude of the metric and thus the greater is the risk to forests. Secondly, the O_3 stress is cumulated over the plant growing season to reflect the time-period when plants are most likely to absorb O_3. In addition, both accumulation periods and critical levels are species-specific reflecting different sensitivities to O_3. Finally, the computation of these standards relies on the concentrations only; therefore they are neither computationally demanding nor expensive in terms of *in-situ* measurements. Similarly, these standards have the same flaw, namely, they do not consider any environmental stress to vegetation, and the risk posed to forests is based on the exposure only without considering any ecophysiological constraint (Anav et al., 2016).

To overcome the above-mentioned flaw, a second group of O_3-risk metric has been developed; this is based on the cumulated stomatal flux above a given phytotoxic threshold below which plants are able to detoxify O_3 (Emberson et al., 2000). The stomatal flux-based metric better reflects the current knowledge on the risk for forests which is based on the amount of pollutant absorbed by the plants through stomata, taking also into account the detoxification processes (Mills et al., 2018). The core of this method is the computation of stomatal conductance, which is based on the Jarvis (1976) multiplicative approach. In the Jarvis model, a prescribed species-specific maximum stomatal conductance is multiplied by several limiting functions and each function takes into account a particular climatic condition which decreases the potential maximum stomatal conductance (Wesely, 1989; Emberson et al., 2000; Clifton et al., 2020). Therefore, the flux-based metric has the capacity of accounting for environmental conditions that influence the O_3 uptake through stomatal aperture (Emberson et al., 2000), thus its use is relevant in circumstances where either high O_3 concentrations are associated with environmental conditions that are unfavourable to uptake (e.g. drought) or low concentrations are associated with mild and wet conditions (Anav et al., 2016).

Given the limitation of exposure-based metrics and the greater biological relevance of flux-based metric, the European Union is considering to replace the AOT40 with a new standard based on stomatal flux of O_3 and expressed as the Phytotoxic Ozone Dose (POD_Y), where Y represents a detoxification threshold below which it is assumed that any ozone molecule absorbed by the leaves will be detoxified (Musselman et al., 2006). For forest protection, this threshold has been set to a constant value of 1 mmol O_3 m^{-2} s^{-1} (CLRTAP, 2017), however it should be noted that this threshold should vary with vegetation type/-species (Mills et al., 2011b).

While at regional scale the spatial and temporal consistency between the different metrics has already been discussed (e.g. Emberson et al., 2000; Simpson et al., 2007; Karlsson et al., 2007; Klingberg et al., 2014; Anav et al., 2016, 2019; De Marco et al., 2020), an assessment at larger scale is still missing for forest ecosystems or is limited to sites where

ozone is measured. In this latter case, however, because of the difficulties associated to the POD_1 computation, which requires several meteorological measurements to be computed, previous comparisons were limited to the exposure-based metrics only (e.g. Lefohn et al., 2018; Mills et al., 2018).

The spatial distribution of AOT40 and W126 is fairly similar, with both standards showing a latitudinal gradient with values increasing from tropics to mid-latitudes and then decreasing toward the high latitudes (Fig. 3); the highest values for AOT40 and W126 are found in the area of higher O_3 concentrations (Fig. 1), namely in mountainous regions and over the polluted areas of eastern China, eastern US and over south Europe. In contrast, the POD_1 shows a more fragmented pattern with maximum values reflecting the combined effect of ozone concentration and meteorological variables. Specifically, the highest POD_1 values are evident in areas where ozone concentrations are not particularly high but have an optimal combination of mild temperatures and scarce soil water stress. Despite these metrics have a different spatial distribution, our results suggest that when used for risk assessment these standards provide a similar picture: in particular, looking at the stipples (Fig. 3), which help to highlight areas where the critical levels for a given metrics are exceeded, the AOT40 shows that critical levels for forest protection are exceeded in the whole US (excluding Alaska), Europe (excluding part of Scandinavian region) and Asia (excluding some regions over the Siberia). Generally, the W126 agrees with this pattern, highlighting the same forests as the most exposed to ozone injury, except a large part of northern Russia and Europe. Similarly, the POD_1 shows the same areas as suggested by W126 and AOT40 even if the risk posed to the forest is less spread compared to other standards: in particular, the POD_1 identifies a large risk over eastern China and India, Mediterranean basin and most of France, as well as east coast of US and

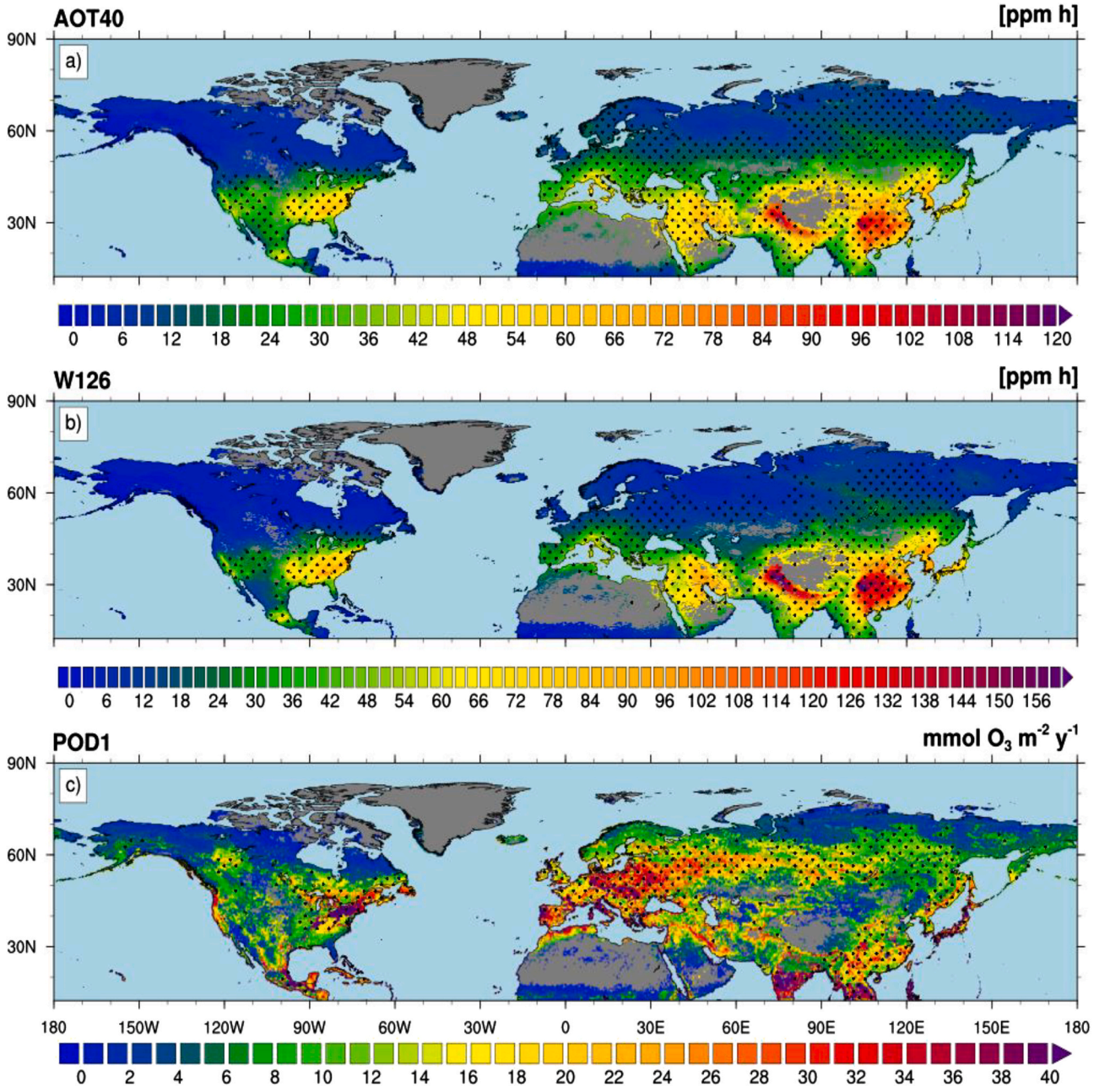

Fig. 3. Standards used or proposed for use in Europe and United States. **a** Spatial distribution of the actual European standard used to protect vegetation from O_3 (AOT40). **b** Metric proposed for use as a secondary air quality standard in the US (W126). **c** Metric proposed in Europe to replace the actual standard. Stipples indicate grid points where critical levels are exceeded.

Mexico.

To fully understand the different spatial pattern of Fig. 3, the differences in the instantaneous (i.e. hourly) values of these metrics should be considered. Fig. 4 suggests that for the concentration-based metrics (i.e. AOT40 and W126), the instantaneous risk to vegetation is a step function of O_3 concentration, irrespective of the stomatal status and hence of any environmental condition. In addition, for the AOT40, all the concentrations below the threshold of 40 ppb are not considered harmful to vegetation, even at high stomatal conductance values. This is also valid for the W126 metrics, however, unlike AOT40, the continuous sigmoidal weighting scheme does not create an artificially imposed concentration threshold. In contrast, the POD_1 shows that the risk depends both on O_3 concentration and stomatal conductance. Specifically, the magnitude of POD_1 is dependent not only on O_3 concentration but also on the variation in the meteorological conditions and plant health status (e.g. phenology, soil moisture, temperature, light, relative humidity, wind speed), which affect the O_3 stomatal conductance and, thus, all control the amount of O_3 entering into the leaves (CLRTAP, 2017). Looking at the POD_1 magnitude, this metric is practically insensitive to variations in O_3 concentrations when stomatal conductance is low (generally below 30 mmol m^{-2} h^{-1}); such insensitivity tends to decrease as the stomatal conductance increases. This behaviour of POD_1 has profound consequences when the metric is used for vegetation adapted to live in limiting climatic conditions such as the Mediterranean and dry or semi-arid environments, which cover 41% of Earth's land surface (Reynolds et al., 2007). In fact, under these conditions, the plant species can adjust their gaseous exchanges to limit the water losses from leaf tissues and then maintain their degree of internal hydration close to optimal conditions. This prevents O_3 to penetrate within the leaf tissues and, therefore, low values of O_3 uptake are observed, regardless of surface O_3 concentration.

Furthermore, Fig. 4 highlights that the dynamics of O_3 uptake are not linearly dependent on O_3 concentrations, therefore the spatial patterns of concentration-based and flux-based metric are significantly different, as shown in Fig. 3. As concentration-based metrics depend on O_3 concentrations only, it is interesting to determine the main drivers controlling the uptake of O_3 at hemispheric level. The spatial distribution of main climatic constraints to stomatal conductance is shown Fig. 5a; in the Arctic region and around the Tibetan plateau and Alps, air temperature is the dominant climate driver controlling stomatal conductance, while it is not surprising that in the boreal region light availability is the strongest constraint controlling, among the other things, stomatal opening. At mid-latitudes and over Africa the water availability represents the main driver for stomatal behaviour, whereas air humidity is the

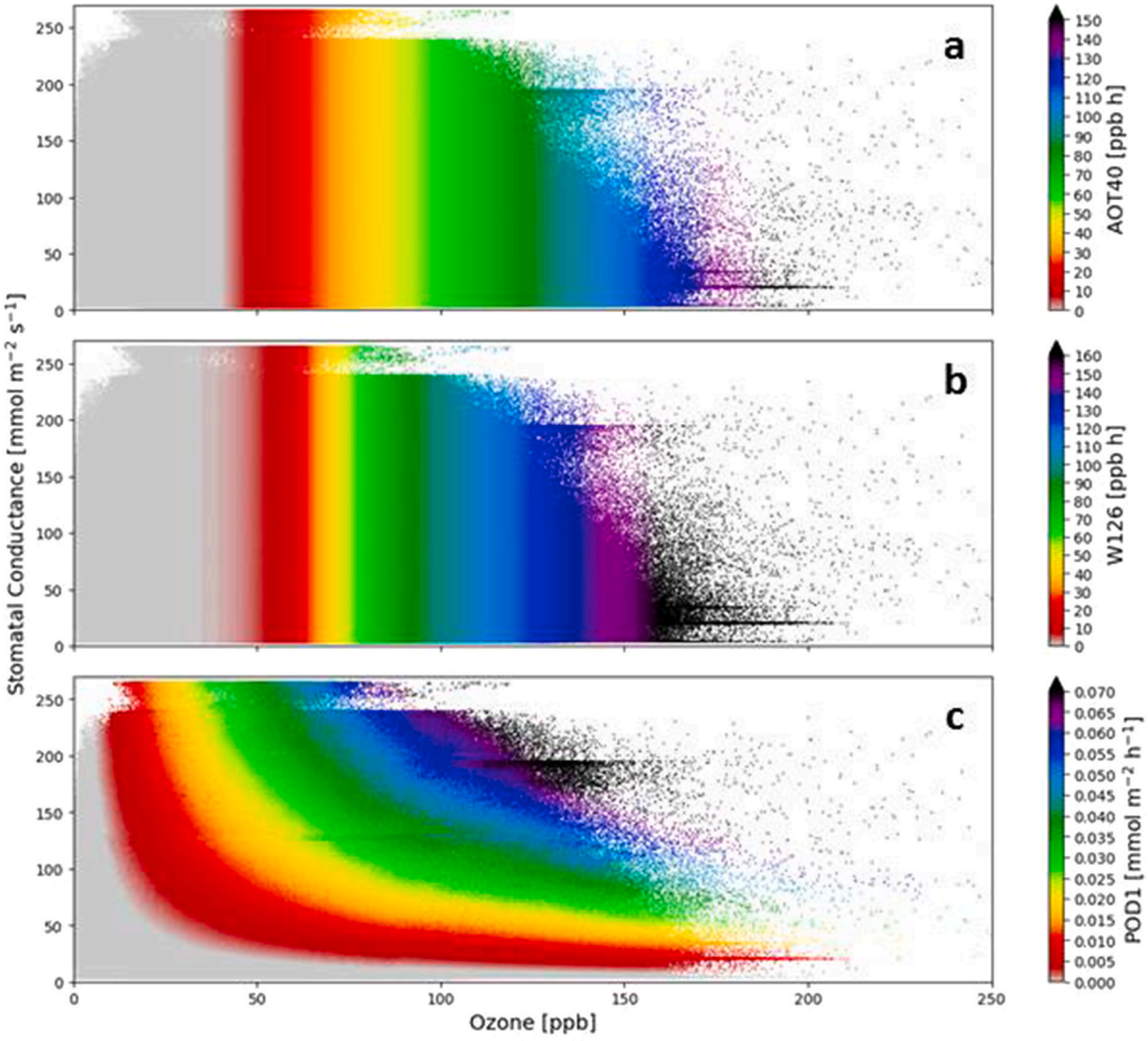

Fig. 4. *Comparison of instantaneous O_3 risk to forests based on AOT40 (a), W126 (b) and POD_1(c). Each dot represents the hourly AOT40, POD_1 and W126 value at one grid point of the model domain during the temporal period June-July-August.*

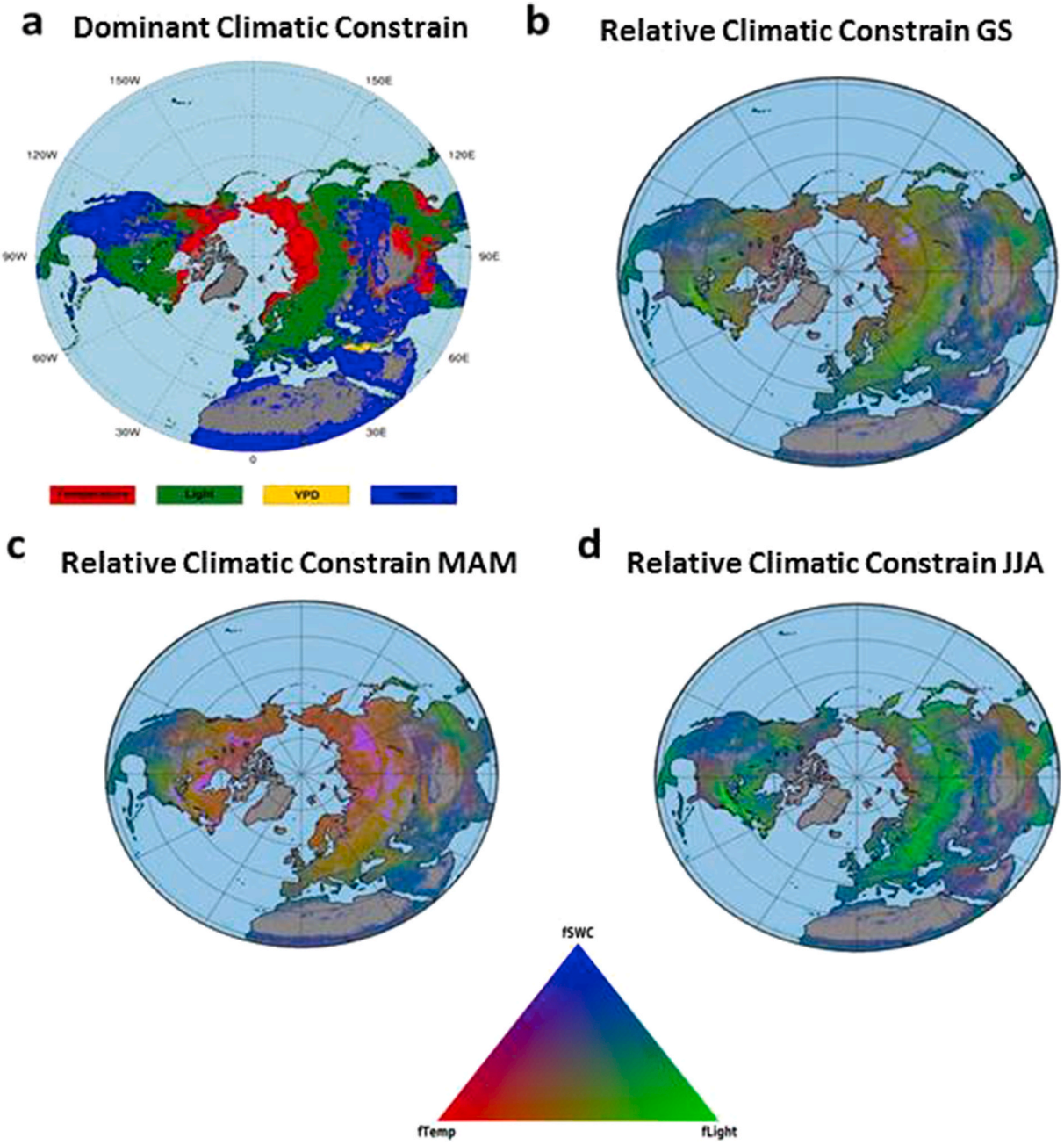

Fig. 5. a: Spatial distribution of dominant meteorological constraints describing the decrease of maximum stomatal conductance with surface air temperature, solar radiation, air humidity (defined as Vapour Pressure Deficit) and soil moisture; consistently with air quality standards, the dominant constraints are computed during plant growing season (April–September) following the Jarvis (1976) multiplicative model. The relative contribution of main constraints limiting stomatal conductance during **b:** plant growing season (April–September) **c:** spring (March-April-May) **d:** summer (June-July-August).

strongest constraint only in a small area over Asia. However, as these constraints could be co-dominant and vary during the year, the seasonal variability caused by each climate driver (i.e., temperature, radiation and soil moisture) is also analyzed. Considering the plant growing season (Fig. 5b), in the boreal region the ozone uptake is co-limited by air temperature and light availability, in the Arctic region temperature has a larger control on stomatal opening, while temperate and sub-tropical regions water and light availability largely control the stomatal conductance. Conversely, when two seasonal periods Spring (March-April-May) and summer (June-July-August) are considered this picture is remarkably different. Air temperature is the dominant constraint from mid to high latitudes, while solar radiation is the strongest constrain in the sub-tropical area, usually characterized by large water availability during the spring period (Fig. 5c). In contrast, during summer (Fig. 5d), because of rising temperature, the daylight becomes the most important factor affecting ozone uptake by plants from mid to high latitudes, while in semi-arid regions water availability plays a pivotal role in regulating stomatal opening. Noteworthy, our results match well the distribution of dominant climatic constraints to plant growth (Nemani et al., 2003) and primary production (Piao et al., 2009; Anav et al., 2015; Wu et al., 2017).

3.3. Process-based models

The metrics described in the above section provide a general picture of risk assessment, but to translate this information into a quantification

of the potential damage to vegetation one should apply 1) dose-response relationships or 2) process-based models.

Process-based models have been extensively used to study the processes leading to either carbon loss or gain by the land ecosystems (Ciais et al., 2014), including the effects of O_3 exposure to forests (Ren et al., 2007; Sitch et al., 2007; Anav et al., 2011; Lombardozzi et al., 2012; Yue et al., 2015; Franz et al., 2017; Unger et al., 2020). These models allow simulating plant responses to varying climate and CO_2 conditions, taking also into account other limiting factors such as nutrient availability, water stress, plant competition and other disturbances (e.g. fires, ozone oxidative stress, insect pests and land use change).

The first observed consequence of elevated levels of O_3 exposure is a decline in net photosynthesis resulting in a reduced growth and hence a reduced leaf area and plant biomass (Wittig et al., 2009); in most of process-based models photosynthesis is simulated following the biochemical model of Farquhar et al. (1980) as modified by Collatz et al. (1991) and others (Anav et al., 2015). In particular, photosynthesis is tightly coupled to stomatal conductance, as stomatal aperture simultaneously affects the exchange of CO_2 and water loss at the leaf surface (Clifton et al., 2020). The Ball-Berry stomatal conductance model (Ball et al., 1987; Collatz et al., 1991) is commonly used in models to simulate stomatal conductance (e.g. Anav et al., 2012); this empirical model uses photosynthetic rates to predict conductance values, hence changes in photosynthesis imply a direct change in stomatal conductance. While this approach is reliable under optimal environmental conditions, photosynthesis and stomatal conductance are shown to become decoupled under oxidative stress caused by ozone (Paoletti and Grulke, 2005; Lombardozzi et al., 2015), thus changing the relationship between gases uptake and water loss (Lombardozzi et al., 2012). Lombardozzi et al. (2012) indicated that vegetation models using Farquhar-von Caemmerer and Berry coupled with the Ball-Berry stomatal model to simulate the ozone damage overestimate the decreases in stomatal conductance, resulting in a large uncertainty in simulated transpiration, latent heat flux and water cycling (Lombardozzi et al., 2015).

The spatial distributions of mean annual GPP, as simulated by ORCHIDEE for the year 2016 with and without considering the effect of O_3, is shown in Fig. 6. The two simulations show a common spatial pattern with a typical longitudinal gradient in Northern Eurasia with GPP decreasing toward the East as a consequence of increasingly continental climate (Beer et al., 2010; Anav et al., 2015). However, it is noteworthy that some remarkable differences in GPP magnitude exist in correspondence of area showing high O_3 concentrations (see Fig. 1): specifically, GPP was reduced by 5% or more in most of Europe (except Spain and Scandinavia), South East Asia and eastern US, where ozone-induced GPP reductions peaks 30%, while in the remaining areas the low ambient [O_3] cannot induce substantial damage. The total GPP simulated with and without O_3 stress is 66.6 PgC y^{-1} and 69.1 PgC y^{-1}, respectively, thus O_3 pollution leads to a GPP reduction of 2.4%. The same value, computed over Europe (6.4%), remarkably differs from Anav et al. (2011) which showed a larger GPP reduction (23.6%) over the same region; however, it should be noted that, despite both the simulations were performed with ORCHIDEE, the parameterization of O_3 stress to photosynthesis are different. In addition, while Anav et al. (2011) considered the effects on both forests and crops, here we focus on

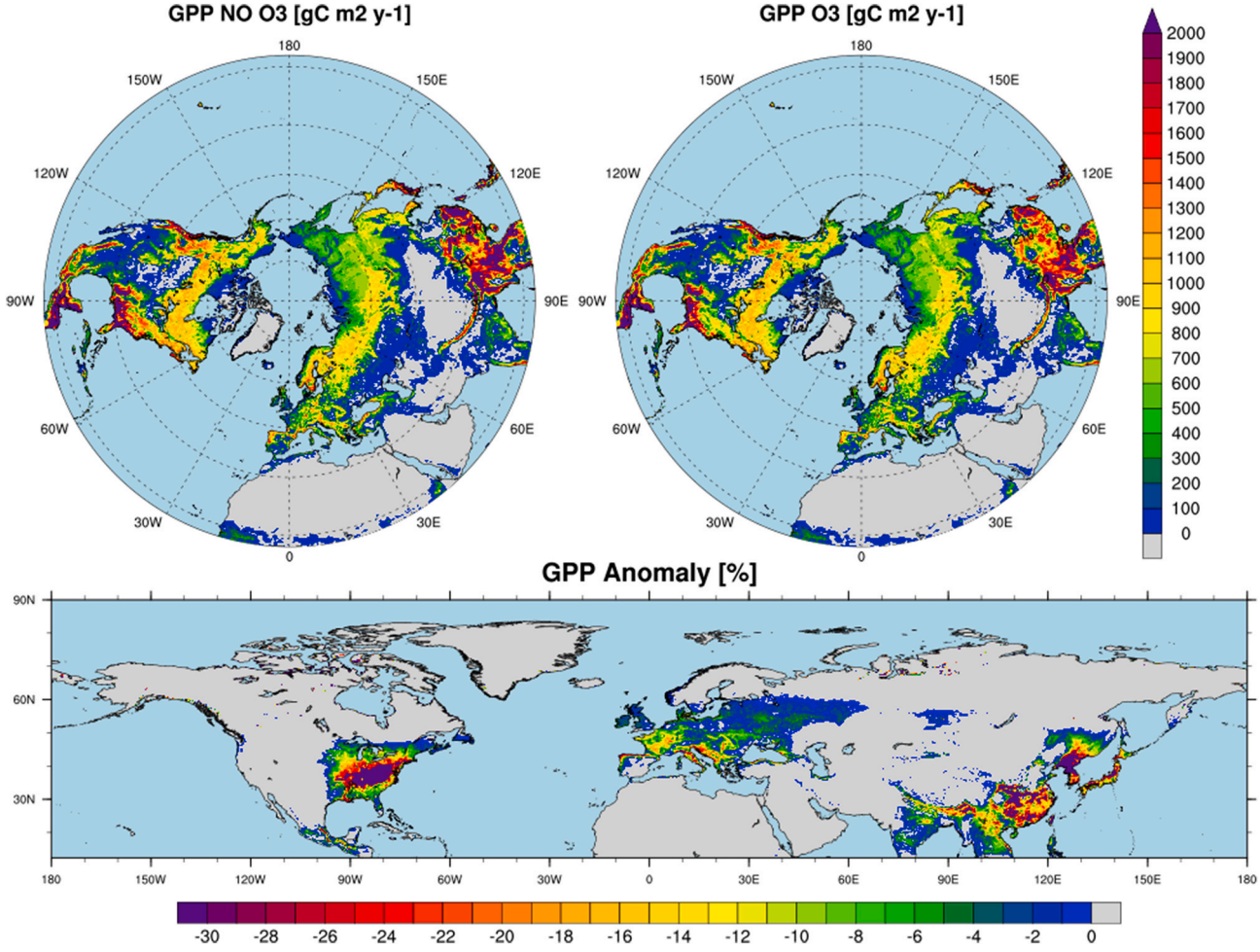

Fig. 6. *Spatial distribution of GPP (forests only) simulated by the ORCHIDEE model with and without considering the ozone stress to vegetation (upper panels). Lower panel shows the annual average GPP losses due to O_3 damage for the year 2016.*

forests only thus this large difference is not surprising as trees are known to possess a defence capacity and can repairing injured tissues, while crops are much more vulnerable (Reich, 1987). Our results well agree with other studies; in particular Yue and Unger (2018) showed exactly the same spatial pattern of GPP reduction of this study, with maxima up to 30%. They concluded that O_3 damages are likely overestimated because of the high biases in modeled O_3 and overall they found a global GPP reduction of 2.9 ± 1.4%. Similarly, Lombardozzi et al. (2015) reported a global GPP decrease of 10.8% in response to O_3 with the largest percent reductions ranging between 20% and 25% with largest reductions occurring in the same areas of this study. More recently, Unger et al. (2020) reported a global GPP reduction of 3.2%, pointing out to Eastern China (−13%), Eastern US (−11%) and Europe (−9%) as the three regions suffering the largest O_3-induced GPP losses. Overall, all these studies, performed with different process-based models and parameterizations of O_3-damage to GPP, agree both in terms of magnitude and identification of the most vulnerable regions to large O_3 stress, despite some differences likely due to differences in the study periods and plant sensitivities to O_3. Nevertheless, the relevant O_3-induced GPP reduction suggests that O_3 plays a pivotal role, more than previously expected, in the land carbon cycle and that it should be taken into account in climate change mitigation studies (Unger et al., 2020). For instance, extreme drought-induced loss of ecosystem function could impact 0.9% ± 0.1% of Earth's vegetated land per year and reduce carbon uptake by 0.14 ± 0.03 PgC yr^{-1} (Du et al., 2018).

4. Conclusions

We analyzed the different European and US legislative standards currently used to protect forests from O_3 in a test case over the northern hemisphere, where forests are known to be potentially more sensitive to ozone damage. In parallel, we described the processes controlling these metrics, identifying the possible sources causing their disagreement.

Results highlighted a similar spatial pattern between AOT40 and W126, while POD_1 showed a different spatial distribution. The similarities between the concentration-based metrics (i.e. AOT40 and W126) are not surprising as these standards are function of O_3 concentration only, while previous studies already showed significant differences in the spatial distribution between AOT40 and PODY over Europe. However, despite the spatial distribution between exposure-based and flux-based metrics is remarkably different, all the standards, associated with their critical levels, provide similar information pointing out the same areas as the most vulnerable to O_3 damage. In addition, the risk computed through the legislative standards agrees, in terms of hot spot regions, with the actual damage estimated using a complex process-based model. This latter result is particularly relevant suggesting that scientists and policy makers can obtain similar information on most vulnerable regions to O_3 damage using tools of different complexity. A major difference among the metrics is in the amount of forests exposed to O3 risk as they exceed the critical level. In detail, AOT40 and W126 suggest that 46% and 61% of the forests in the northern hemisphere are vulnerable to O3 injury, while POD_1 suggests a lower – but still considerable – extent i.e. 40%. Such extent of O3 risk translates into an annual reduction of 2.4% in the forest GPP, which implies significant ecological and economic impacts and suggest that O_3 is a major global threat to forest growth and carbon sequestration.

Vegetation damage by O_3 has widespread consequences, including GPP reduction, decreased land carbon sink, and, ultimately, the amplification of climate change. Thus scientific knowledge must be better communicated to policy makers so that air quality standards adequately protect forests from O_3 threat. Although process-based models will provide the most reliable information about forest vulnerability, this method is perhaps overly complicated for use in air quality standards. We illustrated that POD_1 is the most reliable simple estimate of O_3 risk and recommend this metric is used by policy makers as air quality standard to protect vulnerable forest ecosystems in the future.

Author contributions

AA designed the structure, NV and TV contributed to model set up, AA, ADM, MV, PS prepared a first draft of the manuscript, ADM, AC, ZZ, PS and EP critically revised the manuscript. All authors revised the manuscript for important intellectual content and approved the final version for submission.

Declaration of competing interest

The authors declare that they have no known competing financial interests or personal relationships that could have appeared to influence the work reported in this paper.

Acknowledgements

The authors would like to thank the ECMWF who freely distribute the ERA5 dataset. The computing resources and the related technical support used for this work have been provided by CRESCO/ENEA-GRID High Performance Computing infrastructure and its staff (http://www.cresco.enea.it). CRESCO/ENEAGRID High Performance Computing infrastructure is funded by ENEA, the Italian National Agency for New Technologies, Energy and Sustainable Economic Development and by National and European research programs. Financial support from the LIFE15 ENV/IT/000183 project MOTTLES of the European Union. This work was carried out within the IUFRO Research Group 8.04.00 "Air Pollution and Climate Change".

Appendix A. Supplementary data

Supplementary data to this article can be found online at https://doi.org/10.1016/j.envpol.2021.118690.

References

Agathokleous, E., Saitanis, C.J., Wang, X., Watanabe, M., Koike, T., 2016. A review study on past 40 years of research on effects of tropospheric O 3 on belowground structure, functioning, and processes of trees: a linkage with potential ecological implications. Water, Air, Soil Pollut. 227, 33.

Ainsworth, E.A., Yendrek, C.R., Sitch, S., Collins, W.J., Emberson, L.D., 2012. The effects of tropospheric ozone on net primary productivity and implications for climate change. Annu. Rev. Plant Biol. 63, 637–661.

Anav, A., De Marco, A., Friedlingstein, P., et al., 2019. Growing season extension affects ozone uptake by European forests. Sci. Total Environ. 669, 1043–1052.

Anav, A., De Marco, A., Proietti, C., et al., 2016. Comparing concentration-based (AOT40) and stomatal uptake (PODY) metrics for ozone risk assessment to European forests. Global Change Biol. 22, 1608–1627.

Anav, A., Liu, Q., De Marco, A., Proietti, C., Savi, F., Paoletti, E., Piao, S., 2018. The role of plant phenology in stomatal ozone flux modeling. Global Change Biol. 24, 235–248.

Anav, A., Menut, L., Khvorostyanov, D., Viovy, N., 2011. Impact of tropospheric ozone on the Euro-Mediterranean vegetation. Global Change Biol. 17, 2342–2359.

Anav, A., Menut, L., Khvorostyanov, D., Viovy, N., 2012. A comparison of two canopy conductance parameterizations to quantify the interactions between surface ozone and vegetation over Europe. J. Geophys. Res.: Biogeosciences 117.

Andreae, M.O., Merlet, P., 2001. Emission of trace gases and aerosols from biomass burning. Global Biogeochem. Cycles 15, 955–966.

Ashmore, M., Emberson, L., Karlsson, P.E., Pleijel, H., 2004. New directions: a new generation of ozone critical levels for the protection of vegetation in Europe. Atmos. Environ. 38, 2213–2214.

Ball, J.T., Woodrow, I.E., Berry, J.A., 1987. A model predicting stomatal conductance and its contribution to the control of photosynthesis under different environmental conditions. In: Progress in Photosynthesis Research. Springer.

Beer, C., Reichstein, M., Tomelleri, E., et al., 2010. Terrestrial gross carbon dioxide uptake: global distribution and covariation with climate. Science 329, 834–838.

Braun, S., Schindler, C., Rihm, B., 2014. Growth losses in Swiss forests caused by ozone: epidemiological data analysis of stem increment of Fagus sylvatica L. and Picea abies Karst. Environ. Pollut. 192, 129–138.

Cailleret, M., Ferretti, M., Gessler, A., Rigling, A., Schaub, M., 2018. Ozone effects on European forest growth—towards an integrative approach. J. Ecol. 106, 1377–1389.

Chen, F., Dudhia, J., 2001. Coupling an advanced land surface–hydrology model with the Penn State–NCAR MM5 modeling system. Part I: model implementation and sensitivity. Mon. Weather Rev. 129, 569–585.

Chin, M., Rood, R.B., Lin, S.J., Müller, J.F., Thompson, A.M., 2000. Atmospheric sulfur cycle simulated in the global model GOCART: model description and global properties. J. Geophys. Res. Atmos. 105, 24671–24687.
Ciais, P., Sabine, C., Bala, G., et al., 2014. Carbon and other biogeochemical cycles. In: Climate Change 2013: the Physical Science Basis. Contribution of Working Group I to the Fifth Assessment Report of the Intergovernmental Panel on Climate Change. Cambridge University Press.
Clifton, O.E., Fiore, A.M., Massman, W.J., et al., 2020. Dry Deposition of Ozone over Land: Processes, Measurement, and Modeling. Reviews of Geophysics, e2019RG000670.
CLRTAP, 2017. Mapping Critical Levels for Vegetation, Chapter III of Manual on Methodologies and Criteria for Modelling and Mapping Critical Loads and Levels and Air Pollution Effects, Risks and Trends.
Colette, A., Granier, C., Hodnebrog, Ø., et al., 2012. Future air quality in Europe: a multi-model assessment of projected exposure to ozone. Atmos. Chem. Phys. 12, 10613–10630.
Collatz, G.J., Ball, J.T., Grivet, C., Berry, J.A., 1991. Physiological and environmental regulation of stomatal conductance, photosynthesis and transpiration: a model that includes a laminar boundary layer. Agric. For. Meteorol. 54, 107–136.
Cuesta, J., Kanaya, Y., Takigawa, M., et al., 2018. Transboundary ozone pollution across East Asia: daily evolution and photochemical production analysed by IASI+ GOME2 multispectral satellite observations and models. Atmos. Chem. Phys. 18, 9499–9525.
de Leeuw, F.A., 2000. Trends in ground level ozone concentrations in the European Union. Environ. Sci. Pol. 3 (4), 189e199.
De Marco, A., Sicard, P., Vitale, M., Carriero, G., Renou, C., Paoletti, E., 2015. Metrics of ozone risk assessment for Southern European forests: canopy moisture content as a potential plant response indicator. Atmos. Environ. 120, 182–190.
De Marco, A., Anav, A., Sicard, P., Feng, Z., Paoletti, E., 2020. High Spatial Resolution Ozone Risk-Assessment for Asian Forests Environmental Research Letters, vol. 15, p. 104095.
Doherty, R.M., Stevenson, D.S., Collins, W.J., Sanderson, M.G., 2005. Influence of convective transport on tropospheric ozone and its precursors in a chemistry-climate model. Atmos. Chem. Phys. 5, 3205–3218.
Du, L., Mikle, N., Zou, Z., Huang, Y., Shi, Z., Jiang, L., McCarthy, H.R., Liang, J., Luo, Y., 2018. Global patterns of extreme drought-induced loss in land primary production: identifying ecological extremes from rain-use efficiency. Sci. Total Environ. 628–629, 611–620.
Emberson, L., Ashmore, M., Cambridge, H., Simpson, D., Tuovinen, J.-P., 2000. Modelling stomatal ozone flux across Europe. Environ. Pollut. 109, 403–413.
Emmons, L.K., Walters, S., Hess, P.G., et al., 2010. Description and evaluation of the model for ozone and related chemical Tracers, version 4 (MOZART-4). Geosci. Model Dev. (GMD) 3, 43–67.
EPA US, 2007. Review of the National Ambient Air Quality Standards for Ozone: Policy Assessment of Scientific and Technical Information (OAQPS Staff Paper). Office of Air Quality Planning and Standards.
Fares, S., Vargas, R., Detto, M., Goldstein, A.H., Karlik, J., Paoletti, E., Vitale, M., 2013. Tropospheric ozone reduces carbon assimilation in trees: estimates from analysis of continuous flux measurements. Global Change Biol. 19, 2427–2443.
Farquhar, G.D., Von Caemmerer, S.V., Berry, J.A., 1980. A biochemical model of photosynthetic CO 2 assimilation in leaves of C 3 species. Planta 149, 78–90.
Fischer, E., Jacob, D.J., Yantosca, R.M., et al., 2014. Atmospheric peroxyacetyl nitrate (PAN): a global budget and source attribution. Atmos. Chem. Phys. 14, 2679–2698.
Forzieri, G., Girardello, M., Ceccherini, G., et al., 2021. Emergent vulnerability to climate-driven disturbances in European forests. Nat. Commun. 12, 1081.
Franz, M., Alonso, R., Arneth, A., et al., 2018. Evaluation of simulated ozone effects in forest ecosystems against biomass damage estimates from fumigation experiments. Biogeosciences 15, 6941–6957.
Franz, M., Simpson, D., Arneth, A., Zaehle, S., 2017. Development and evaluation of an ozone deposition scheme for coupling to a terrestrial biosphere model. Biogeosciences 14, 45–71.
Fuhrer, J., Skärby, L., Ashmore, M.R., 1997. Critical levels for ozone effects on vegetation in Europe. Environ. Pollut. 97, 91–106.
Fuhrer, J., Val Martin, M., Mills, G., et al., 2016. Current and future ozone risks to global terrestrial biodiversity and ecosystem processes. Ecol. Evol. 6, 8785–8799.
Gaudel, A., Cooper, O., Ancellet, G., et al., 2018. Tropospheric Ozone Assessment Report: Present-Day Distribution and Trends of Tropospheric Ozone Relevant to Climate and Global Atmospheric Chemistry Model Evaluation.
Georgiou, G.K., Christoudias, T., Proestos, Y., Kushta, J., Hadjinicolaou, P., Lelieveld, J., 2018. Air quality modelling in the summer over the eastern Mediterranean using WRF-Chem: chemistry and aerosol mechanism intercomparison. Atmos. Chem. Phys. 18, 1555–1571.
Grell, G.A., Peckham, S.E., Schmitz, R., Mckeen, S.A., Frost, G., Skamarock, W.C., Eder, B., 2005. Fully coupled "online" chemistry within the WRF model. Atmos. Environ. 39, 6957–6975.
Guenther, A., Karl, T., Harley, P., Wiedinmyer, C., Palmer, P.I., Geron, C., 2006. Estimates of global terrestrial isoprene emissions using MEGAN (Model of emissions of gases and aerosols from nature) Atmos. Chem. Phys. 6, 3181–3210.
Guo, D., Su, Y., Shi, C., Xu, J., Powell, A.M., 2015. Double core of ozone valley over the Tibetan Plateau and its possible mechanisms. J. Atmos. Sol. Terr. Phys. 130–131, 127–131.
Hartmann, D.L., Tank, A.M.K., Rusticucci, M., et al., 2013. Observations: atmosphere and surface. In: Climate Change 2013 the Physical Science Basis: Working Group I Contribution to the Fifth Assessment Report of the Intergovernmental Panel on Climate Change. Cambridge University Press.
Heath, R.L., Lefohn, A.S., Musselman, R.C., 2009. Temporal processes that contribute to nonlinearity in vegetation responses to ozone exposure and dose. Atmos. Environ. 43, 2919–2928.
Hersbach, H., Bell, B., Berrisford, P., Hirahara, S., Horányi, A., Muñoz-Sabater, J., et al., 2020. The ERA5 global reanalysis. Q. J. R. Meteorol. Soc. 146, 1999–2049.
Hong, S.-Y., Lim, J.-O.J., 2006. The WRF single-moment 6-class microphysics scheme (WSM6). Asia-Pacific Journal of Atmospheric Sciences 42, 129–151.
Hoshika, Y., Katata, G., Deushi, M., Watanabe, M., Koike, T., Paoletti, E., 2015. Ozone-induced stomatal sluggishness changes carbon and water balance of temperate deciduous forests. Sci. Rep. 5, 9871.
Hoshika, Y., Omasa, K., Paoletti, E., 2012. Whole-tree water use efficiency is decreased by ambient ozone and not affected by O3-induced stomatal sluggishness. PLoS One 7, e39270.
Huang, M., Carmichael, G.R., Pierce, R.B., et al., 2017. Impact of intercontinental pollution transport on North American ozone air pollution: an HTAP phase 2 multi-model study. Atmos. Chem. Phys. 17, 5721–5750.
Iacono, M.J., Delamere, J.S., Mlawer, E.J., Shephard, M.W., Clough, S.A., Collins, W.D., 2008. Radiative forcing by long-lived greenhouse gases: calculations with the AER radiative transfer models. J. Geophys. Res. Atmos. 113.
Jarvis, P., 1976. The interpretation of the variations in leaf water potential and stomatal conductance found in canopies in the field. Philos. Trans. R. Soc. Lond. B Biol. Sci. 273, 593–610.
Johnson, A.H., Siccama, T.G., 1983. Acid deposition and forest decline. Environ. Sci. Technol. 17, 294A–305A.
Jolivet, Y., Bagard, M., Cabané, M., et al., 2016. Deciphering the ozone-induced changes in cellular processes: a prerequisite for ozone risk assessment at the tree and forest levels. Ann. For. Sci. 73, 923–943.
Jonson, J.E., Schulz, M., Emmons, L., et al., 2018. The effects of intercontinental emission sources on European air pollution levels. Atmos. Chem. Phys. Discuss. https://doi.org/10.5194/acp-2018-79 (submitted for publication).
Karlsson, P., Braun, S., Broadmeadow, M., et al., 2007. Risk assessments for forest trees: the performance of the ozone flux versus the AOT concepts. Environ. Pollut. 146, 608–616.
Kitao, M., Yasuda, Y., Kominami, Y., et al., 2016. Increased phytotoxic O 3 dose accelerates autumn senescence in an O 3-sensitive beech forest even under the present-level O 3. Sci. Rep. 6, 32549.
Klingberg, J., Engardt, M., Karlsson, P.E., Langner, J., Pleijel, H., 2014. Declining ozone exposure of European vegetation under climate change and reduced precursor emissions. Biogeosciences 11, 5269–5283.
Kottek, M., Grieser, J., Beck, C., Rudolf, B., Rubel, F., 2006. World map of the Köppen-Geiger climate classification updated. Meteorol. Z. 15, 259–263.
Krinner, G., Viovy, N., De Noblet-Ducoudré, N., et al., 2005. A dynamic global vegetation model for studies of the coupled atmosphere-biosphere system. Global Biogeochem. Cycles 19.
Kronfuß, G., Polle, A., Tausz, M., Havranek, W., Wieser, G., 1998. Effects of ozone and mild drought stress on gas exchange, antioxidants and chloroplast pigments in current-year needles of young Norway spruce [Picea abies (L.) Karst.]. Trees (Berl.) 12, 482–489.
Lamarque, J.-F., Shindell, D.T., Josse, B., et al., 2013. The Atmospheric Chemistry and Climate Model Intercomparison Project (ACCMIP): overview and description of models, simulations and climate diagnostics. Geosci. Model Dev. (GMD) 6, 179–206.
Law, K.S., Stohl, A., 2007. Arctic air pollution: origins and impacts. Science 315, 1537–1540.
Lefohn, A.S., Malley, C.S., Smith, L., et al., 2018. Tropospheric Ozone Assessment Report: Global Ozone Metrics for Climate Change, Human Health, and Crop/ecosystem Research.
Leisner, C.P., Ainsworth, E.A., 2012. Quantifying the effects of ozone on plant reproductive growth and development. Global Change Biol. 18, 606–616.
Li, P., Feng, Z., Catalayud, V., Yuan, X., Xu, Y., Paoletti, E., 2017. A meta-analysis on growth, physiological, and biochemical responses of woody species to ground-level ozone highlights the role of plant functional types. Plant Cell Environ. 40, 2369–2380.
Li, X., Liu, J., Mauzerall, D.L., Emmons, L.K., Walters, S., Horowitz, L.W., Tao, S., 2014. Effects of trans-Eurasian transport of air pollutants on surface ozone concentrations over Western China. J. Geophys. Res. Atmos. 119, 12,338–12,354.
Lin, M., Fiore, A.M., Horowitz, L.W., et al., 2012. Transport of Asian ozone pollution into surface air over the western United States in spring. J. Geophys. Res. Atmos. 117.
Lombardozzi, D., Levis, S., Bonan, G., Hess, P., Sparks, J., 2015. The influence of chronic ozone exposure on global carbon and water cycles. J. Clim. 28, 292–305.
Lombardozzi, D., Levis, S., Bonan, G., Sparks, J., 2012. Predicting photosynthesis and transpiration responses to ozone: decoupling modeled photosynthesis and stomatal conductance. Biogeosci. Discuss. 9.
Lombardozzi, D., Sparks, J., Bonan, G., 2013. Integrating O 3 influences on terrestrial processes: photosynthetic and stomatal response data available for regional and global modeling. Biogeosciences 10, 6815–6831.
Loveland, T.R., Reed, B.C., Brown, J.F., Ohlen, D.O., Zhu, Z., Yang, L., Merchant, J.W., 2000. Development of a global land cover characteristics database and IGBP DISCover from 1 km AVHRR data. Int. J. Rem. Sens. 21, 1303–1330.
Matyssek, R., Karnosky, D., Wieser, G., et al., 2010a. Advances in understanding ozone impact on forest trees: messages from novel phytotron and free-air fumigation studies. Environ. Pollut. 158, 1990–2006.
Matyssek, R., Wieser, G., Ceulemans, R., et al., 2010b. Enhanced ozone strongly reduces carbon sink strength of adult beech (Fagus sylvatica)–Resume from the free-air fumigation study at Kranzberg Forest. Environ. Pollut. 158, 2527–2532.

Mavrakis, A., Flocas, H.A., Mavromatidis, E., Kallos, G., Theoharatos, G., Christides, A., 2010c. A case of nighttime high ozone concentration over the greater Athens area. Meteorol. Z. 19, 35–45.
Milford, J.B., Gao, D., Sillman, S., Blossey, P., Russell, A.G., 1994. Total reactive nitrogen (NO y) as an indicator of the sensitivity of ozone to reductions in hydrocarbon and NO x emissions. J. Geophys. Res. Atmos. 99, 3533–3542.
Mills, G., Hayes, F., Simpson, D., Emberson, L., Norris, D., Harmens, H., Büker, P., 2011a. Evidence of widespread effects of ozone on crops and (semi-) natural vegetation in Europe (1990–2006) in relation to AOT40-and flux-based risk maps. Global Change Biol. 17, 592–613.
Mills, G., Pleijel, H., Braun, S., et al., 2011b. New stomatal flux-based critical levels for ozone effects on vegetation. Atmos. Environ. 45, 5064–5068.
Mills, G., Pleijel, H., Malley, C., et al., 2018. Tropospheric ozone assessment report: present day tropospheric ozone distribution and trends relevant to vegetation. Elem Sci Anth 6, 47.
Monks, P.S., Archibald, A., Colette, A., et al., 2015. Tropospheric ozone and its precursors from the urban to the global scale from air quality to short-lived climate forcer. Atmos. Chem. Phys. 15, 8889–8973.
Musselman, R.C., Lefohn, A.S., Massman, W.J., Heath, R.L., 2006. A critical review and analysis of the use of exposure-and flux-based ozone indices for predicting vegetation effects. Atmos. Environ. 40, 1869–1888.
Nemani, R.R., Keeling, C.D., Hashimoto, H., et al., 2003. Climate-driven increases in global terrestrial net primary production from 1982 to 1999. Science 300, 1560–1563.
Novak, K., Schaub, M., Fuhrer, J., et al., 2005. Seasonal trends in reduced leaf gas exchange and ozone-induced foliar injury in three ozone sensitive woody plant species. Environ. Pollut. 136, 33–45.
Oikonomakis, E., Aksoyoglu, S., Ciarelli, G., Baltensperger, U., Prévôt, H., Stephan, A., 2018. Low modeled ozone production suggests underestimation of precursor emissions (especially NO x) in Europe. Atmos. Chem. Phys. 18.
Oliver, R.J., Mercado, L.M., Sitch, S., Simpson, D., Medlyn, B.E., Lin, Y.-S., Folberth, G. A., 2018. Large but decreasing effect of ozone on the European carbon sink. Biogeosciences 15, 4245–4269.
Paoletti, E., De Marco, A., Beddows, D.C., Harrison, R.M., Manning, W.J., 2014. Ozone levels in European and USA cities are increasing more than at rural sites, while peak values are decreasing. Environ. Pollut. 192, 295–299.
Paoletti, E., De Marco, A., Racalbuto, S., 2007. Why should we calculate complex indices of ozone exposure? Results from Mediterranean background sites. Environ. Monit. Assess. 128, 19–30.
Paoletti, E., Grulke, N.E., 2005. Does living in elevated CO2 ameliorate tree response to ozone? A review on stomatal responses. Environ. Pollut. 137, 483–493.
Park, J.H., Lee, D.K., Gan, J., et al., 2018. Effects of climate change and ozone concentration on the net primary productivity of forests in South Korea. Forests 9, 112.
Parrish, D.D., Law, K.S., Staehelin, J., Derwent, R., Cooper, O.R., Tanimoto, H., Volz-Thomas, A., Gilge, S., Scheel, H.-E., Steinbacher, M., Chan, E., 2013. Lower tropospheric ozone at northern midlatitudes: changing seasonal cycle, Geophys. Res. Lett. 40, 1631–1636.
Parrish, D., Lamarque, J.F., Naik, V., et al., 2014. Long-term changes in lower tropospheric baseline ozone concentrations: comparing chemistry-climate models and observations at northern midlatitudes. J. Geophys. Res. Atmos. 119, 5719–5736.
Pell, E., Eckardt, N., Enyedi, A., 1992. Timing of ozone stress and resulting status of ribulose bisphosphate carboxylase/oxygenase and associated net photosynthesis. New Phytol. 120, 397–405.
Piao, S., Ciais, P., Friedlingstein, P., De Noblet-Ducoudré, N., Cadule, P., Viovy, N., Wang, T., 2009. Spatiotemporal patterns of terrestrial carbon cycle during the 20th century. Global Biogeochem. Cycles 23.
Pretzsch, H., Dieler, J., Matyssek, R., Wipfler, P., 2010. Tree and stand growth of mature Norway spruce and European beech under long-term ozone fumigation. Environ. Pollut. 158, 1061–1070.
Proietti, C., Anav, A., De Marco, A., Sicard, P., Vitale, M., 2016. A multi-sites analysis on the ozone effects on Gross Primary Production of European forests. Sci. Total Environ. 556, 1–11.
Reich, P.B., 1987. Quantifying plant response to ozone: a unifying theory. Tree Physiol. 3, 63–91.
Reich, P.B., Amundson, R.G., 1985. Ambient levels of ozone reduce net photosynthesis in tree and crop species. Science 230, 566–570.
Ren, W., Tian, H., Liu, M., et al., 2007. Effects of tropospheric ozone pollution on net primary productivity and carbon storage in terrestrial ecosystems of China. J. Geophys. Res. Atmos. 112.
Reynolds, J.F., Smith, D.M.S., Lambin, E.F., et al., 2007. Global desertification: building a science for dryland development. Science 316, 847–851.
Rydsaa, J.H., Stordal, F., Gerosa, G., Finco, A., Hodnebrog, Ø., 2016. Evaluating stomatal ozone fluxes in WRF-Chem: comparing ozone uptake in Mediterranean ecosystems. Atmos. Environ. 143, 237–248.
Schultz, M.G., Schröder, S., Lyapina, O., et al., 2017. Tropospheric Ozone Assessment Report: database and metrics data of global surface ozone observations. Elementa: Science of the Anthropocene 5.
Sicard, P., Anav, A., Marco, A.D., Paoletti, E., 2017. Projected global ground-level ozone impacts on vegetation under different emission and climate scenarios. Atmos. Chem. Phys. 17, 12177–12196.
Sicard, P., De Marco, A., Dalstein-Richier, L., Tagliaferro, F., Renou, C., Paoletti, E., 2016. An epidemiological assessment of stomatal ozone flux-based critical levels for visible ozone injury in Southern European forests. Sci. Total Environ. 541, 729–741.
Simpson, D., Ashmore, M., Emberson, L., Tuovinen, J.-P., 2007. A comparison of two different approaches for mapping potential ozone damage to vegetation. A model study. Environ. Pollut. 146, 715–725.
Sitch, S., Cox, P., Collins, W., Huntingford, C., 2007. Indirect radiative forcing of climate change through ozone effects on the land-carbon sink. Nature 448, 791.
Skamarock, W.C., Klemp, J.B., 2008. A time-split nonhydrostatic atmospheric model for weather research and forecasting applications. J. Comput. Phys. 227, 3465–3485.
Sofen, E., Bowdalo, D., Evans, M., 2016a. How to most effectively expand the global surface ozone observing network. Atmos. Chem. Phys. 1445–1457.
Sofen, E., Bowdalo, D., Evans, M., et al., 2016b. Gridded global surface ozone metrics for atmospheric chemistry model evaluation. Earth Syst. Sci. Data 41–59.
Strode, S.A., Rodriguez, J.M., Logan, J.A., et al., 2015. Trends and variability in surface ozone over the United States. J. Geophys. Res. Atmos. 120, 9020–9042.
Sun, G., Mclaughlin, S.B., Porter, J.H., Uddling, J., Mulholland, P.J., Adams, M.B., Pederson, N., 2012. Interactive influences of ozone and climate on streamflow of forested watersheds. Global Change Biol. 18, 3395–3409.
Talhelm, A.F., Pregitzer, K.S., Kubiske, M.E., et al., 2014. Elevated carbon dioxide and ozone alter productivity and ecosystem carbon content in northern temperate forests. Global Change Biol. 20, 2492–2504.
Tarasick, D., Galbally, I.E., Cooper, O.R., et al., 2019. Tropospheric Ozone Assessment Report: tropospheric ozone from 1877 to 2016, observed levels, trends and uncertainties. Elem Sci Anth 7.
Tian, W., Chipperfield, M., Huang, Q., 2008. Effects of the Tibetan Plateau on total column ozone distribution. Tellus B 60 (4), 622–635.
Unger, N., Zheng, Y., Yue, X., Harper, K.L., 2020. Mitigation of ozone damage to the world's land ecosystems by source sector. Nat. Clim. Change 1–4.
Verryckt, L.T., Beeck, M.O.D., Neirynck, J., Gielen, B., Roland, M., Janssens, I.A., 2017. No impact of tropospheric ozone on the gross primary productivity of a Belgian pine forest. Biogeosciences 14, 1839–1855.
Walker, T.W., Jones, D.B.A., Parrington, M., Henze, D.K., Murray, L.T., Bottenheim, J.W., Anlauf, K., Worden, J.R., Bowman, K.W., Shim, C., Singh, K., Kopacz, M., Tarasick, D.W., Davies, J., von der Gathen, P., Thompson, A.M., Carouge, C.C., 2012. Impacts of midlatitude precursor emissions and local photochemistry on ozone abundances in the arctic. J. Geophys. Res. Atmos. 117.
Wang, L., Pang, J., Feng, Z., Zhu, J., Kobayashi, K., 2015. Diurnal variation of apoplastic ascorbate in winter wheat leaves in relation to ozone detoxification. Environ. Pollut. 207, 413–419.
Wesely, M., 1989. Parameterization of surface resistances to gaseous dry deposition in regional-scale numerical models. Atmos. Environ. 23, 1293–1304.
Wiedinmyer, C., Akagi, S., Yokelson, R.J., Emmons, L., Al-Saadi, J., Orlando, J., Soja, A., 2011. The Fire INventory from NCAR (FINN): a high resolution global model to estimate the emissions from open burning. Geosci. Model Dev. (GMD) 4, 625.
Wittig, V.E., Ainsworth, E.A., Naidu, S.L., Karnosky, D.F., Long, S.P., 2009. Quantifying the impact of current and future tropospheric ozone on tree biomass, growth, physiology and biochemistry: a quantitative meta-analysis. Global Change Biol. 15, 396–424.
Wu, Z., Ahlström, A., Smith, B., Ardö, J., Eklundh, L., Fensholt, R., Lehsten, V., 2017. Climate data induced uncertainty in model-based estimations of terrestrial primary productivity. Environ. Res. Lett. 12, 064013.
Young, P., Archibald, A., Bowman, K., et al., 2013. Pre-industrial to end 21st century projections of tropospheric ozone from the atmospheric chemistry and climate model intercomparison project (ACCMIP). Atmos. Chem. Phys. 13, 2063–2090.
Yue, X., Keenan, T.F., Munger, W., Unger, N., 2016. Limited effect of ozone reductions on the 20-year photosynthesis trend at Harvard forest. Global Change Biol. 22, 3750–3759.
Yue, X., Unger, N., 2014. Ozone vegetation damage effects on gross primary productivity in the United States. Atmos. Chem. Phys. 14, 9137–9153.
Yue, X., Unger, N., 2018. Fire air pollution reduces global terrestrial productivity. Nat. Commun. 9, 1–9.
Yue, X., Unger, N., Harper, K., et al., 2017. Ozone and haze pollution weakens net primary productivity in China. Atmos. Chem. Phys.
Zhang, C., Wang, Y., Hamilton, K., 2011. Improved representation of boundary layer clouds over the southeast Pacific in ARW-WRF using a modified Tiedtke cumulus parameterization scheme. Mon. Weather Rev. 139, 3489–3513.